Dynamics of optical vortices in 2D materials

Yaniv Kurman
Technion - Israel Institute of Technology https://orcid.org/0000-0002-5784-3573
Raphael Dahan
Technion, Israel Institute of Technology
Hanan Herzig Sheinfux
Institute of Photonic Sciences
Gilles Rosolen
University of Mons
Eli Janzen
Kansas State University
James Edgar
Kansas State University https://orcid.org/0000-0003-0918-5964
Frank Koppens
ICFO - The Institute of Photonic Sciences https://orcid.org/0000-0001-9764-6120
Ido Kaminer (kaminer@technion.ac.il)
Technion - Israel Institute of Technology https://orcid.org/0000-0003-2691-1892

Article

Keywords:

Posted Date: January 14th, 2022

DOI: https://doi.org/10.21203/rs.3.rs-1234204/v1

Dynamics of optical vortices in 2D materials

Yaniv Kurman[1], Raphael Dahan[1], Hanan Herzig Shenfux[2], Gilles Rosolen[3], Eli Janzen[4], James H. Edgar[4], Frank H. L. Koppens[2,5], and Ido Kaminer[1*]

[1]Department of Electrical Engineering, Technion, Israel Institute of Technology, 32000 Haifa, Israel

[2]ICFO-Institut de Ciències Fotòniques, The Barcelona Institute of Science and Technology, Av. Carl Friedrich Gauss 3, 08860 Castelldefels (Barcelona), Spain

[3]Micro and Nanophotonic Materials Group, Research Institute for Materials Science and Engineering, University of Mons, 7000 Mons, Belgium

[4]Tim Taylor Department of Chemical Engineering, Kansas State University, Manhattan, KS 66506 USA

[5]ICREA-Institució Catalana de Recerca i Estudis Avanats, Passeig Lluís Companys 23, 08010 Barcelona, Spain

*Correspondence to: kaminer@technion.ac.il

Optical vortices in planar geometries are a universal wave phenomenon, where electromagnetic waves possess topologically protected integer values of orbital angular momentum (OAM). The conservation of OAM governs their dynamics, including their rules of creation and annihilation. However, such dynamics remained so far beyond experimental reach. Here, we present a first observation of creation and annihilation of optical vortex pairs. The vortices conserve their combined OAM during pair creation/annihilation events and determine the field profile throughout their motion between these events. We utilize free electrons in an ultrafast transmission electron microscope to probe the vortices, which appear in the form of phonon polaritons in the 2D material hexagonal boron nitride. These results provide the first observation of optical vortices in any 2D material, which were predicted but never observed. Our findings promote future investigation of vortices in 2D materials and their use for chiral plasmonics, toward the control of selection rules in light-matter interactions and the creation of optical simulators of phase transitions in condensed matter physics.

Optical vortices are points in the light field with non-zero optical orbital angular momentum (OAM) [1]. In these points, the phase is undefined, creating a singularity with zero amplitude and integer values of OAM which equals the integrated phase of the field (over 2π) in a closed contour around the vortex location [2, 3]. Distinguished by dimensionality, two distinct families of optical vortices are known: vortex beams [4] and planar vortices [5]. Vortex beams showed a plethora of phenomena [6] from stimulated emission depletion (STED) microscopy [7] and optical tweezers [8], through nonlinear optical effects such as vortex solitons [9], to implications for quantum entanglement [10,11] and transfer of angular momentum from light to matter [12].

In planar systems, optical vortices are confined to the 2D-plane and evanescently decay in the out-of-plane direction, as famously shown with surface plasmon polaritons [5] and with other guided modes [13]. Their reduced dimensionality led to unique phenomena such as nanotweezers [14], optical skyrmions [15], and manipulation of selection rules in light-matter interactions [16, 17]. Much of the research on 2D optical vortices is focused on controlling the vortex OAM and location [18-20]. The control is primarily based on engineering the boundary conditions and the laser excitation properties (e.g., polarization), even showing vortices with high OAM [21]. Delicate engineering of the interference of planar waves enabled sub-cycle ultrafast observations of the formation, dissipation, and rotation of individual vortices [21-24] and of topological plasmon vortices (and vortex arrays), as optical analogous to magnetic merons and skyrmions [23, 24]. The latter works suggested to use active control of the excitation pulses to "enable the creation, manipulation and annihilation of plasmonic topological spin textures" [23].

Fundamental to the physics of vortices is the conservation of their topological OAM, implying that vortex pairs can be created or annihilated while maintaining a fixed overall OAM in

each process [25]. These conservation laws were probed experimentally by sweeping over the frequency [26] or polarization [20] of time harmonic (monochromatic) fields. These approaches provide an indirect analogue of the temporal dynamics of vortices, showing that pairs of vortices can be created and annihilated, and change their location for slowly varying continuous wave fields [27].

The creation and annihilation of vortices are of particular interest in ultrafast optics: ultrafast optical phenomena require a wide bandwidth of frequency components and while each component separately can support vortices in a different location, their constructive interference is expected to destroy the vortices by eliminating their phase singularities. Thus, the conservation laws that exist in each individual frequency component might be broken for ultrafast dynamics. To the best of our knowledge, no work so far accessed the full spatiotemporal dynamics of optical vortices, to show the in-plane motion of a vortex and its evolution from creation to annihilation.

In this work, we observe the spatiotemporal dynamics of 2D optical vortices, identifying events of vortex-pair creation and annihilation. The 2D optical vortices appear as points of zero field amplitude that are shown to move continuously inside the sample. All the features predicted by the theory of vortex temporal dynamics (Fig. 1) are found in our experiments. The OAM of individual vortices is conserved during their movement and the combined OAM is conserved during the creation and annihilation of vortex pairs when inside the bulk. However, the OAM is not conserved on sample edges. Our experiment promotes ideas for optical simulators of exotic spatiotemporal phenomena in condensed matter physics, such as the Berezinskii–Kosterlitz–Thouless (BKT) phase transition [28].

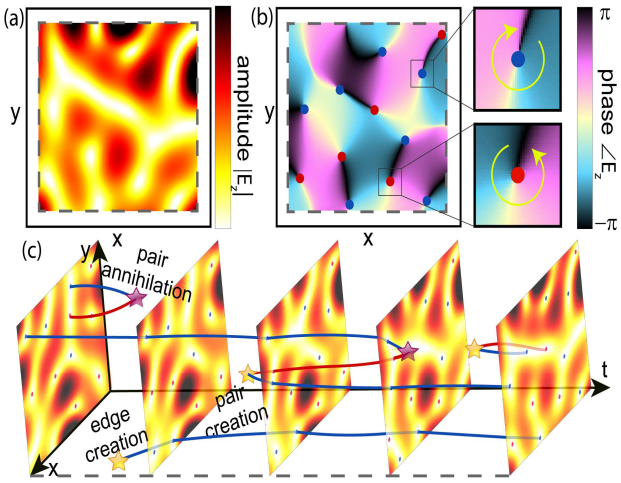

Figure 1: Theory of 2D optical vortex dynamics. Exemplified by a simulation of phonon-polaritons (PhP) in hexagonal boron nitride (hBN). **(a)** Simulated PhP electric field amplitude $|E_z|$. **(b)** The corresponding phase of the field, from which we can determine the locations of the vortices. The vortex locations match the amplitude nodal points. Inset: The blue and red dots denote the location of the left-handed and right-handed vortices, respectively. **(c)** The electric field amplitude as a function of time, marking a few vortex trajectories (blue and red curves) and creation\annihilation events (stars).

We use an ultrafast transmission electron microscope (UTEM) [29-35] to probe the spatiotemporal dynamics of the phonon polariton (PhP) vortices in boron-10 isotopically pure hexagonal boron nitride ($h^{10}BN$). hBN is a widely studied 2D material which exhibits unique hyperbolic PhPs [36-42]. Besides PhPs in hBN, 2D materials span a much larger range of polaritons (including plasmon-polariton, phonon-polariton, exciton-polariton, and more [43, 44]), which have dispersion relations that may be tuned via their thicknesses, surrounding environments, and material doping. Here, PhPs were chosen due to their slow group velocity that determined the vortex velocity and the relatively long lifetime of the PhPs in monoisotopic boron $h^{10}BN$ in room temperature [38, 42]. The long lifetime was essential for showing other 2D optical phenomena in room temperature such as PhP cavity dynamics [39], wavepacket dynamics [41], and PhP lensing [40]. Our observation of PhP vortices in hBN is the first measurement of optical vortices in any 2D-polaritonic system.

Spatiotemporal imaging of 2D vortices using free electrons

Fig. 2 shows how we extract the temporal dynamics of the vortices. We use a pump-probe technique, in which a single laser pulse is divided so that one part is converted to the mid infrared (IR) regime to pump the PhPs in the sample, while the other part is converted to the UV to excite the free electron probe in the UTEM (see details in SM section S1). Our probing approach is based on the technique called photon-induced near-field electron microscopy (PINEM) [29], which originally operated in the visible and near IR range [30-35]. The pulsed free electron interacts with the electric field along its trajectory, resulting in a widening of its energy spectrum. The image of the PhPs is produced when applying an energy filter which collects only the electrons that gained energy from their interaction with the PhPs. This technique is named energy-filtered transmission electron microscopy (EFTEM) [45-47]. The filtering creates a threshold for the minimum electric field that we can measure. Above this threshold, there is a quadratic connection between the integrated electric field along the electron trajectory and the number of counts in the image [30, 31]. The dynamics of the field is probed when changing the time delay τ_d between the mid-IR pump pulse and the free-electron probe pulse. A similar approach to observe field spatiotemporal dynamics was first used in [41] to monitor the propagation of PhP wavepackets and extract their group velocities. We use time steps of 50 fs and find vortex dynamics for a duration of 4.5 ps, significantly longer than the mid IR pulse duration of 600 fs FWHM.

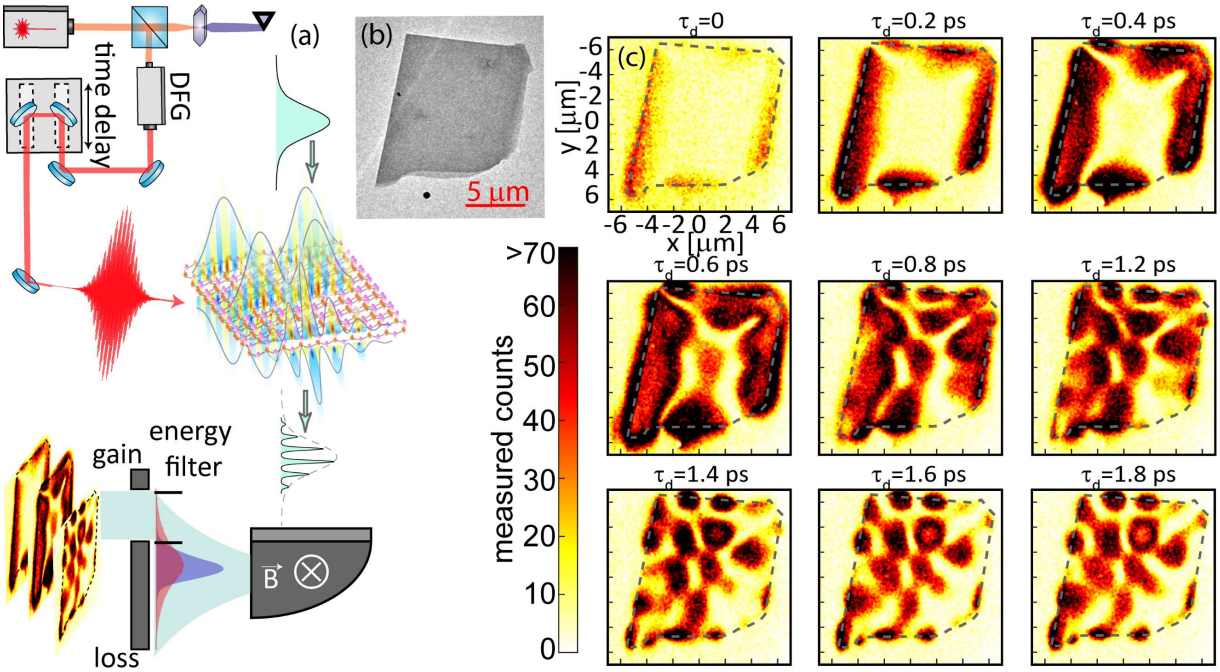

Figure 2: Experimental setup and measurement examples showing spatiotemporal dynamics of optical vortices. (a) Experimental setup. A femtosecond laser pulse (orange) splits in two. One pulse serves as the pump, converted to the mid-infrared (IR; red) using difference frequency generation (DFG) and excites the phonon-polaritons (PhPs) in the sample. The other pulse is converted to ultraviolet (UV; purple) using fourth harmonic generation (FHG) and photoexcites the electron probe pulse (cyan). We image the PhP field in the hBN by energy filtering, counting only electrons that gained energy. The dynamics is retrieved by changing the time delay τ_d between the pump and the probe. **(b)** TEM image of the 40 nm thick isotopically pure hBN (^{10}B) sample. See SM section S3 and Fig. S4 for a detailed sample analysis. **(c)** PhP field patterns for different time delays, showing the evolution of complex interference pattern dynamics. The dashed gray contour is the sample's edge. The bright areas that include fewer counts are nodal lines and points where vortices are located. The full 3D movie that continues until $\tau_d = 4.5$ ps with 50 fs time steps can be found in Movie S1.

The PhP spatiotemporal dynamics is shown in Fig. 2b and Movie S1. The PhP field is excited at the edges of the sample (coupling directly to the bulk is impossible due to momentum mismatch between the free-space photons and the PhP modes). From the edges, the PhP wavepackets propagate toward the sample center (τ_d=0 to 0.4 ps) and interfere with each other (meeting at the center around τ_d = 0.6 ps). Due to this interference, the measured field pattern fluctuates and changes in a complex manner. Yet, there are a few clear structures that stand out of this fluctuating landscape: nodal points and nodal lines in the PhP field. As shown by our simulations, these features are the signature of PhP vortices. By following the nodal points, we study the vortex dynamics.

Vortex creation and annihilation

In Fig. 3 (and Movie S2), we present an example of the simulated motion of vortex dynamics and their processes of creation and annihilation (thorough description in SM section S2). We simulate a 6×6 μm^2 square hBN sample and analyze both the amplitude and phase of the field in the time domain. Indeed, the nodal points of the field (top row) correspond to the optical vortices that we extract from the phase of the field (bottom row). By following the field map evolution in time, we find specific timestamps in which the vortices are created and annihilated. For further validation of the results, we also performed full electromagnetic COMSOL simulations of the field dynamics, showing that the measured features can be reproduced numerically for a sample shape similar to the one used in the experiment (Figs. S6 and S7).

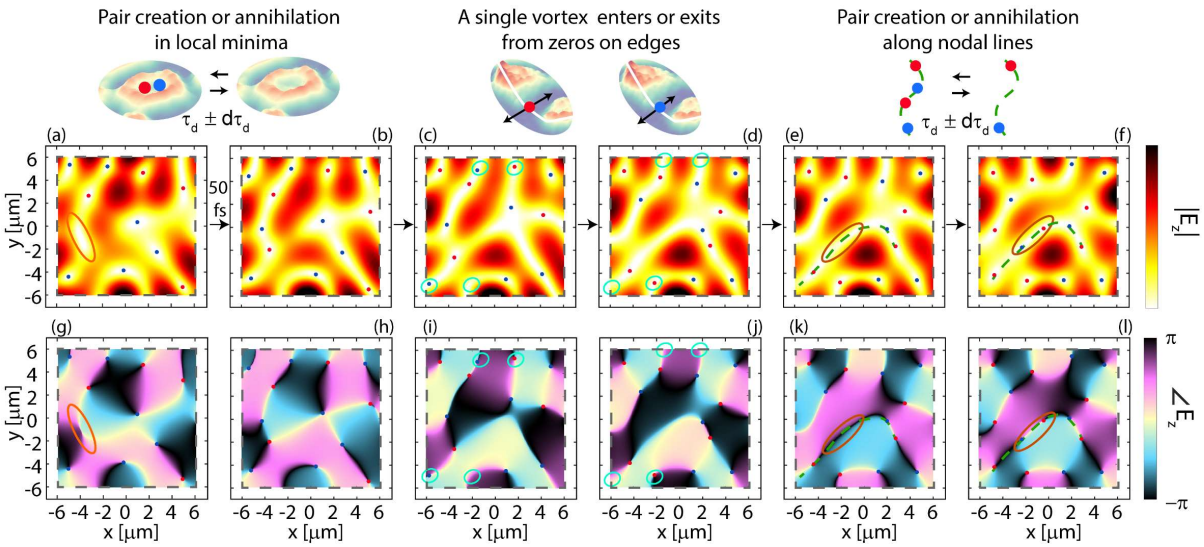

Figure 3: Vortex dynamics, creation, and annihilation. (a-b) A pair of right-handed and left-handed vortices can be created when the field amplitude at a certain point reduces to zero, forming a nodal point, or annihilated if the nodal point suddenly disappears. **(c-d)** A single vortex of any orientation may be created or annihilated on the sample's edge. Thus, both the local OAM and the total OAM within the sample are not conserved. **(e-f)** A pair of vortices can be created or annihilated within nodal lines (dashed green) along which the field amplitude is already near zero. Such nodal lines are formed between at least two vortices with opposite orientations. Often when two vortices are distant from each other, additional vortex pairs are created between them, effectively supporting a longer nodal line. **(g-l)** The phase maps corresponding to images (a)-(f). The time delay between consequent images is 50 fs.

Fig. 3 summarizes the three mechanisms in which vortices are created and annihilated. The first option (Fig. 3 left column) is the creation of a pair of opposite sign vortices, occurring when the amplitude of a certain point reduces to zero. Thus, a non-zero local minima possess a total OAM of zero but has the potential to become the source of a pair of vortices. When such a pair move away from one another, they create a nodal line. Nodal lines appear as continuous curves along which the field is near zero. They are formed by a set of vortices of alternating OAM that destructively interfere.

The second option for the creation or annihilation of a pair of vortices is inside an existing nodal line (Fig. 3 right column). When the distance between neighboring vortices inside a nodal lines grows, another pair of vortices with opposite signs is often created along the nodal line,

maintaining a longer nodal line through their destructive interference. Importantly, in both of the above mechanisms of pair creation, each individual vortex can move inside the sample and annihilate with any vortex of the opposite OAM.

Since pairs of vortices can be created or annihilated, the total number of vortices is not conserved. The quantity that is conserved is the local OAM at each point inside the bulk. However, the total OAM of the field in the sample is not conserved due to a third mechanism of vortex creation and annihilation – along the edges, single vortices can be created or annihilated (Fig. 3 middle column). At the core of this mechanism is the effect of anomalous reflection of planar waves at the edges of the sample that adds a phase to the field [48, 39]. Altering the phase of the field enables phase distortions equivalent to having single vortices enter and exit the sample along the edges. Equivalently, because of the nature of optical vortices [1], the combined OAM of all vortices in the sample equals the integrated phase along the sample edges, and if the phase is changing, a vortex might be created or annihilated. Once a vortex is created on the sample edge it can change its location, annihilate with another vortex of an opposite sign, or annihilate on the edge (usually at a different location from where it was created).

Analysis of the measured spatiotemporal vortex dynamics

Our experimental observation of vortex creation and annihilation demonstrates the features predicted by the theory. Specifically, Fig. 4a shows selected timeframes to highlight vortex dynamics, in close agreement with the theory we showed in Fig. 1: we follow the trajectories of all the vortices in the flake and find that certain trajectories of vortices of opposite signs can begin (end) at certain points in time and space, which correspond to the process of creation (annihilation). The complete measurement including the locations and signs of the vortices in each time frame is shown in Movie S3 and Fig. S1 [49].

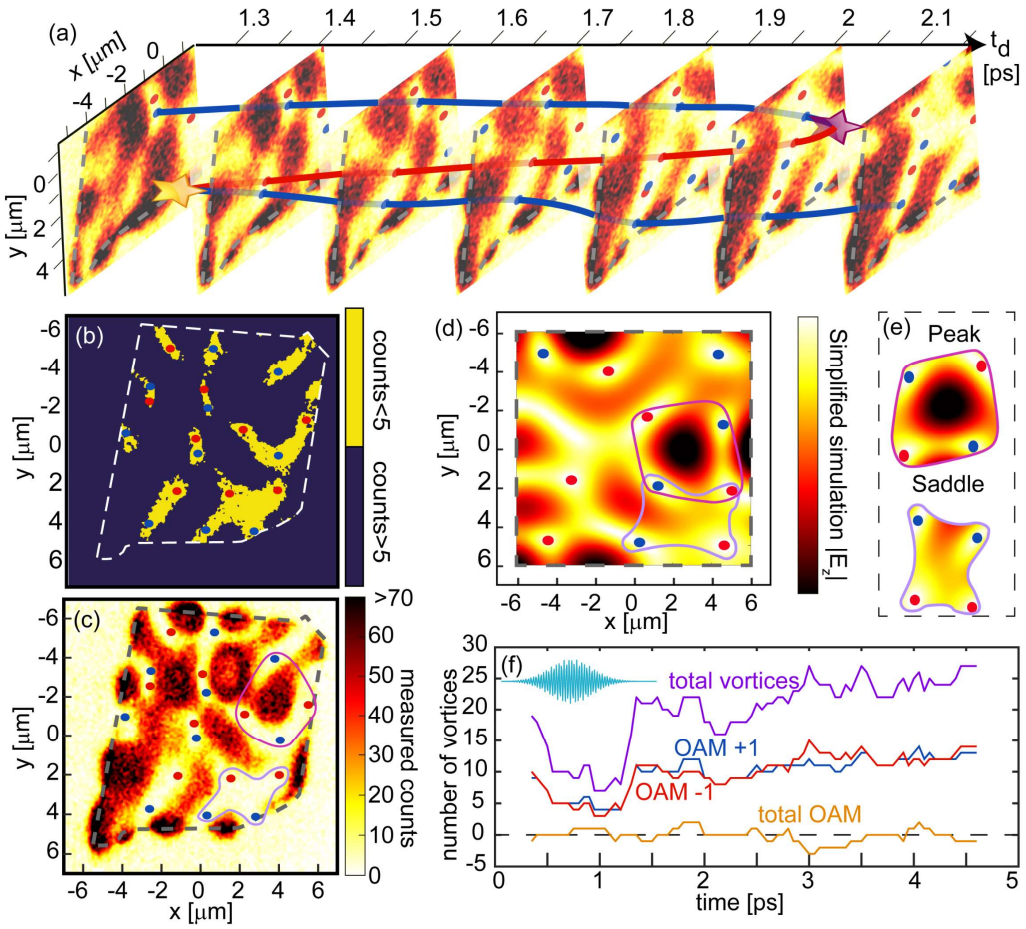

Figure 4: Observation of vortex dynamics. (a) Selected timeframes showing the vortex dynamics, marking events of creation and annihilation. A few vortex trajectories are shown through the blue and red curves: a right-handed (red) vortex is created from a pair creation process at τ_d =1.3 ps and annihilated with a left-handed (blue) vortex at τ_d =2.05 ps. The reconstruction of all vortices throughout our measurement is shown Fig. S1 and Movie S3. **(b)** First step for identification of vortices – areas of nodal points and nodal lines (where optical vortices appear) are denoted in yellow (more information in Fig. S2). **(c)** The experimental measurement for τ_d = 1.8 ps with the estimated vortex locations (up to flipping all vortex orientations). **(d)** The simulation field pattern in a specific timeframe, showing how a set of vortices can determine the qualitative shape of the field's pattern inside the sample. **(e)** An amplitude peak is formed when surrounded by a set of vortices with alternating orientations (pink). When the vortex orientations are not alternating, a saddle point is created, having a smaller amplitude compared to the peak (gray). **(f)** The number of vortices with an OAM of +1 (blue), -1 (red), their sum (purple), and difference (brown). The total OAM changes due to creation or annihilation of vortices on the edges while the total number of vortices includes pair creation or annihilation. The excitation pulse duration is shown in blue. The comparison with a full numerical COMSOL simulation is shown in Fig. S7.

Fig. 4b-e show how we deduce the location and sign of the vortices. For each frame, we find the vortex locations by identifying the nodal points and nodal lines, appearing as areas with extremely low counts (Fig. 4b and Fig. S2). Then, we analyze the field pattern to determine the OAM sign of each vortex (Fig. 4c). We can verify from simulations (Fig. 4d-e) that each peak of the field is surrounded by a set of vortices of alternating signs (e.g., +-+-), forcing a uniformity in the phase within the peak. In contrast, when the vortices do not have alternating signs (e.g., ++--), the field that is surrounded by these vortices is not a peak but a saddle, having a smaller amplitude compared to a peak and a larger variation in the phase inside it. The saddle configuration can create a large area in the sample with very low counts (Fig. 4c bottom right). This area seems to have almost zero counts due to the minimal electric field that we can measure (~1 MV/m, SM section S1), but it is not strictly zero (see the average signal over time, Fig. S3). Finally, when comparing the estimated vortices in all timestamps, we recognize the continuous movement of the vortices and the events of vortex creation and annihilation.

The observation of vortex dynamics shows the prospects of our experimental platform as an optical simulator of hard-to-access spatiotemporal phenomena such as vortex dynamics and phase transitions in condensed matter systems. In these systems, vortex-antivortex correlations exist for a condensate in the low-temperature phase but disappear in the high-temperature phase after a Berezinskii–Kosterlitz–Thouless (BKT) phase transition [28]. In our measurement (Fig. 4f.) and simulations (Fig. S7), we identify the total number of vortices and the total OAM of the flake as a function of time. We observe that the laser excitation (cyan in Fig. 4f) acts as a source of order that decreases the total number of vortices when it is applied on the sample, analogous to reducing the effective temperature in a solid-state BKT-type system. The number of vortices then gradually increase again after the laser excitation is over. The degrees of freedom in controlling

the optical excitations and the system's boundary conditions make planar optical platforms valuable simulators to promote our understanding of condensed-matter physics phenomena (e.g., [15, 23]).

Discussion and outlook

Our experiment stands as an example for the universal nature of planar vortices. In most experiments that showed 2D optical vortices so far, the boundary conditions were designed for generating a specific vortex OAM at a specific location that remains constant in time (e.g., [21, 22]). In our experiment, we used the natural edges of the sample to show that vortex spatiotemporal dynamics can appear in arbitrary samples with only a single requirement – that the sample is optically mesoscopic. We can divide all samples into three categories (see Fig. 5): (1) If the sample's dimensions are smaller than the typical wavelength of the optical modes, it can support only a few modes. The field in such cavity-like samples possess a distinct shape [39] and cannot show vortex dynamics or any complex dynamics. We present an example of such an observation in Fig. 5a. The resonant mode can potentially have a phase singularity forming an optical vortex, but such a vortex cannot have temporal dynamics changing its location in time. (2) On the other extreme, if the sample's dimensions are much larger than the decay length of the optical modes, there is dynamics, but no interference from different boundaries, and thus optical vortices cannot form. This is the case in [41], shown in Fig. 5c, having a wavepacket propagating freely in-plane, moving away from the edge. (3) Consequently, spatiotemporal dynamics of vortices can only occur in samples of intermediate sizes – optically mesoscopic sample – larger than the typical wavelength of the optical modes and smaller than their typical decay length. This is the case in our work, as shown in Fig. 5b.

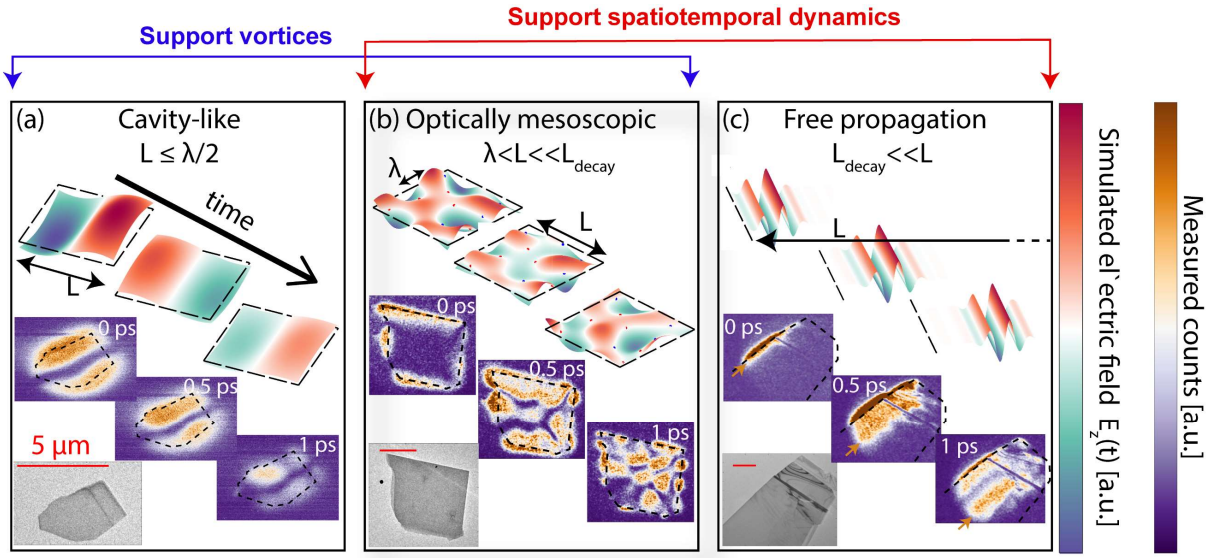

Figure 5: Universality of optical vortex dynamics: 2D optical vortices are expected in any mesoscopic-size sample of arbitrary shape. (a) Small samples: Spatial dimensions (L) much smaller than the wavelength of light in the material (λ). The electric field pattern (both simulated and measured) has a cavity-like mode with no field dynamics. Such samples can support vortices for specific sample shapes, though the location of the vortex is static. **(b)** Optically mesoscopic samples: Spatial dimensions (L) much smaller than the decay length of light in the material (L_{decay}) but larger than the wavelength of light in the material (λ). These conditions are sufficient for having the spatiotemporal dynamics of optical vortices (shown in both simulated and measured plots) in arbitrary sample shapes, due to complex interference patterns that evolve over time. **(c)** Large samples: Spatial dimensions (L) much larger than the decay length of light in the material (L_{decay}). Such dimensions support free-propagation dynamics (data taken from [41]), until the field disperses and decays. In all figures, the dashed lines denote the sample's boundaries. The inset at the bottom of each panel shows a hBN flake of the corresponding size with which the presented data was collected. The red bar denotes 5 μm in all insets.

It is interesting to compare the features of PhP vortices to vortices in exciton-polariton condensates [50]. There, a strong interaction between matter and an optical cavity mode creates the condensate, which can form a superfluid [51]. Previous work in such systems show the creation and propagation of vortex pairs [52, 53] but did not so far measure their spatiotemporal dynamics. Although sharing certain polaritonic properties with PhPs, the behavior of exciton-polaritons arise from the Gross-Pitaevskii equation and requires extremely low temperatures, in contrast to the PhP vortices that arise from Maxwell's equations and were measured here at room temperature. Recent demonstrations of quantum simulations [54] and analogies of gravity [55] with exciton-polaritons

raise intriguing possibilities for similar prospects with PhPs, especially once higher excitation intensities reach the regime where their nonlinear optical response cannot be neglected [56]. It is possible that nonlinear effects had already affected our measurements here (see Fig. S8 and SM section S4). Future investigations may deliberately introduce nonlinearity through atomic emitters or 2D quantum wells, exploiting their extremely strong light–matter interactions with 2D light [57], and specifically with vortices of 2D light [16, 17].

Looking forward, desired vortex phenomena such as studying chiral plasmonics [58] with 2D polaritons could be created by engineering boundary conditions (for example using inverse design methods [59]). Moreover, if excited by non-classical light, a properly designed boundary condition could establish full entanglement between two vortex states of opposite charge (± 1) at two different locations r_1, r_2: taking the form of $|+1, r_1\rangle|-1, r_2\rangle + |-1, r_1\rangle|+1, r_2\rangle$. Together with the precise ultrafast coherent control and deep-subwavelength spatial resolution, 2D material platforms could be suitable for demonstrating and probing wide ranges of vortex phenomena in optics and condensed matter physics.

References

[1] Nye, J. F. & Berry, M. V. Dislocations in wave trains. Proc. R. Soc. Lond. A **336**, 165–190 (1974).

[2] Coullet, P., Gil, L. & Rocca, F. Optical vortices. *Opt. Commun.* **73**, 403–408 (1989).

[3] Soskin, M. S. et al. Topological charge and angular momentum of light beams carrying optical vortices. *Phys. Rev. A* **56**, 4064–4075 (1997).

[4] Allen, L., Beijersbergen, M. W., Spreeuw, R. J. C. & Woerdman, J. P. Orbital angular momentum of light and the transformation of Laguerre–Gaussian laser modes. *Phys. Rev. A* **45**, 8185–8189 (1992).

[5] Gorodetski, Y., Niv, A., Kleiner, V. & Hasman, E. Observation of the spin-based plasmonic effect in nanoscale structures. *Phys. Rev. Lett*. **101**, 043903 (2008).

[6] Shen, Y. et al. Optical vortices 30 years on: OAM manipulation from topological charge to multiple singularities. *Light Sci. Appl.* **8**, 90 (2019).

[7] Willig, K. I. et al. STED microscopy reveals that synaptotagmin remains clustered after synaptic vesicle exocytosis. *Nature* **440**, 935–939 (2006).

[8] Gahagan, K. T. & Swartzlander, G. A. Optical vortex trapping of particles. *Opt. Lett.* **21**, 827–829 (1996).

[9] Swartzlander, G. A. Jr. & Law, C. T. Optical vortex solitons observed in Kerr nonlinear media. *Phys. Rev. Lett.* **69**, 2503–2506 (1992).

[10] Nagali, E. et al. Quantum information transfer from spin to orbital angular momentum of photons. *Phys. Rev. Lett.* **103**, 013601 (2009).

[11] Stav, T. et al. Quantum entanglement of the spin and orbital angular momentum of photons using metamaterials. *Science* **361**, 1101–1104 (2018).

[12] He, H. et al. Direct observation of transfer of angular momentum to absorptive particles from a laser beam with a phase singularity. *Phys. Rev. Lett.* **75**, 826–829 (1995).

[13] Balistreri, M. L. M., Korterik, J. P., Kuipers, L. & van Hulst, N. F. Local observations of phase singularities in optical fields in waveguide structures. *Phys. Rev. Lett.* **85**, 294–297 (2000).

[14] Wang, K., Schonbrun, E., Steinvurzel, P. et al. Trapping and rotating nanoparticles using a plasmonic nano-tweezer with an integrated heat sink. Nat Commun 2, 469 (2011).

[15] Tsesses, S. et al. Optical skyrmion lattice in evanescent electromagnetic fields. *Science* **361**, 993–996 (2018).

[16] Machado, F., Rivera, N., Buljan, H., Soljacic, M. & Kaminer, I. Shaping polaritons to reshape selection rules. *ACS Photon.* **5**, 3064–3072 (2018).

[17] Sloan, J., Rivera, N., Joannopoulos, J. D., Kaminer, I. & Soljacic, M. Controlling spins with surface magnon polaritons. *Phys. Rev. B* **100**, 235453 (2019).

[18] Kim, H. et al. Synthesis and dynamic switching of surface plasmon vortices with plasmonic vortex lens. *Nano Lett*. **10**, 529–536 (2010).

[19] David, A., Gjonaj, B., Blau, Y., Dolev, S. & Bartal, G. Nanoscale shaping and focusing of visible light in planar metal–oxide–silicon waveguides. *Optica* **2**, 1045–1048 (2015).

[20] Ostrovsky, E. et al. Nanoscale control over optical singularities. *Optica* **5**, 283–288 (2018).

[21] Spektor, G. et al. Orbital angular momentum multiplication in plasmonic vortex cavities. *Science Adv.* **7**, eabg5571 (2021).

[22] Spektor, G. et al. Revealing the subfemtosecond dynamics of orbital angular momentum in nanoplasmonic vortices. *Science* **355**, 187–1191 (2017).

[23] Dai, Y. et al. Plasmonic topological quasiparticle on the nanometre and femtosecond scales. *Nature* **588,** 616–619 (2020).

[24] Davis, T. J. et al. Ultrafast vector imaging of plasmonic skyrmion dynamics with deep subwavelength resolution. *Science* **368**, eaba6415 (2020).

[25] Berry, M. V. & Dennis, M. R. Knotted and linked phase singularities in monochromatic waves. *Proc. R. Soc. A* **457**, 2251–2263 (2001).

[26] De Angelis, L., Alpeggiani, F., Di Falco, A., & Kuipers, L. Spatial distribution of phase singularities in optical random vector waves. *Phys. Rev. Lett.* **117**, 093901 (2016).

[27] De Angelis, L., Alpeggiani, F., Di Falco, A., & Kuipers, L. Persistence and lifelong fidelity of phase singularities in optical random waves *Phys. Rev. Lett.* **119**, 203903 (2017).

[28] Kosterlitz, J. M. & Thouless, D. J. Ordering, metastability and phase transitions in twodimensional systems. *J. Phys. C* **6**, 1181–1203 (1973).

[29] Barwick, B., Flannigan, D. J., & Zewail, A. H. Photon-induced near-field electron microscopy. *Nature* **462,** 902 (2009).

[30] García de Abajo, F. J., Asenjo-Garcia, A., & Kociak, M. Multiphoton absorption and emission by interaction of swift electrons with evanescent light fields. *Nano Lett.* **10,** 1859-1863 (2010).

[31] Park, S. T., Lin, M., & Zewail, A. H. Photon-induced near-field electron microscopy (PINEM): theoretical and experimental. *New Journal of Physics* **12,** 123028 (2010).

[32] Lummen, T. et al. Imaging and controlling plasmonic interference fields at buried interfaces. *Nat. Commun.* **7,** 13156 (2016).

[33] Pomarico, E. et al. meV Resolution in laser-assisted energy-filtered transmission electron microscopy. *ACS Photon.* **5**, 759–764 (2018).

[34] Madan, I. et al. Holographic imaging of electromagnetic fields via electron-light quantum interference. *Sci. Adv*. **5**, eaav8358 (2019)

[35] Wang, K. et al. Coherent interaction between free electrons and a photonic cavity. *Nature* **582**, 50–54 (2020).

[36] Dai, S. et al. Tunable phonon polaritons in atomically thin van der Waals crystals of boron nitride. *Science* **343**, 1125–1129 (2014).

[37] Caldwell, J. et al. Sub-diffractional volume-confined polaritons in the natural hyperbolic material hexagonal boron nitride. *Nat. Commun.* **5,** 5221 (2014).

[38] Giles, A. J. et al. Ultralow-loss polaritons in isotopically pure boron nitride. *Nat. Mater*. **17**, 134–139 (2018).

[39] Tamagnone, M. et al. Ultra-confined mid-infrared resonant phonon polaritons in van der Waals nanostructures. *Sci. Adv.* **4**, eaat7189 (2018).

[40] Chaudhary, K. et al. Engineering phonon polaritons in van der Waals heterostructures to enhance in-plane optical anisotropy. *Sci. Adv.* **5**, eaau7171 (2019).

[41] Kurman, Y. et al. Spatiotemporal imaging of 2D polariton wave packet dynamics using free electrons. *Science* **372** 1181-1186 (2021).

[42] Pavlidis, G. et al. Experimental confirmation of long hyperbolic polariton lifetimes in monoisotopic (10B) hexagonal boron nitride at room temperature. *APL Materials* **9**, 091109 (2021).

[43] Basov, D. N., Fogler, M. M. & García de Abajo, F. J. Polaritons in van der Waals materials. *Science* **354**, aag1992 (2016).

[44] Low, T. et al. Polaritons in layered two-dimensional materials. *Nature Mater* **16,** 182–194 (2017).

[45] Egerton, R.F. *Electron Energy-Loss Spectroscopy in the Electron Microscope* **370** (Plenum, New York and London, 1996).

[46] Nelayah, J. et al. Mapping surface plasmons on a single metallic nanoparticle. *Nature Phys.* **3**, 348–353 (2007).

[47] Bosman, M., Keast, V. J., Watanabe, M., Maaroof, A. I. & Cortie, M. B. Mapping surface plasmons at the nanometre scale with an electron beam. *Nanotechnology* **18**, 165505 (2007).

[48] Kang, J. et al. Goos-Hänchen shift and even–odd peak oscillations in edge-reflections of surface polaritons in atomically thin crystals. *Nano Lett.* **17**, 1768–1774 (2017).

[49] We note that our overall vortex reconstruction has a few degrees of freedom that are indistinguishable. For example, if all vortices flip their OAM, the amplitude map that we measure does not change (i.e., we could flip all vortices blue ↔ red). Another unknown is the number of vortices found along nodal lines, since the near-zero amplitude along these lines can potentially sustain arbitrary numbers of degenerate vortices, where each pair has its phase cancelling out.

[50] Lagoudakis, K. G. et al. Quantized vortices in an exciton–polariton condensate. *Nature Phys.* **4**, 706–710 (2008).

[51] Amo, A. et al. Superfluidity of polaritons in semiconductor microcavities. *Nature Phys.* **5**, 805–810 (2009).

[52] Amo, A. et al. Polariton superfluids reveal quantum hydrodynamic solitons. *Science* **332**, 1167–1170 (2011).

[53] Lerario, G. et al. Vortex-stream generation and enhanced propagation in a polariton superfluid. *Phys. Rev. Research* **2**, 023049 (2020).

[54] Boulier, T. et al. Microcavity polaritons for quantum simulation. *Adv. Quantum Technol.* **3**, 2000052 (2020).

[55] Jacquet, M. J. et al. Polariton fluids for analogue gravity physics. *Philosophical Transactions of the Royal Society A* **378**, 20190225 (2020).

[56] Iyikanat, F., Konečná, A., & de Abajo, F. Nonlinear Tunable Vibrational Response in Hexagonal Boron Nitride. *arXiv preprint arXiv:2105.08153* (2021).

[57] Kurman, Y. & Kaminer, I. Tunable bandgap renormalization by nonlocal ultra-strong coupling in nanophotonics. *Nat. Phys.* **16,** 868–874 (2020).

[58] Hentschel, M., Schäferling, M., Duan, X., Giessen, H. & Liu, N. Chiral plasmonics. *Sci. Adv*. **3**, e1602735 (2017).

[59] Piggott, A. Y. et al. Inverse design and demonstration of a compact and broadband on-chip wavelength demultiplexer. *Nature Photon.* **9**, 374–377 (2015).

Supplementary Files

This is a list of supplementary files associated with this preprint. Click to download.

- SM2.pdf
- MovieS2.avi
- MovieS1.avi
- MovieS4.avi
- MovieS3.mp4